An investigation into spray combustion processes of waste cooking oil biodiesel fuel under diesel engine conditions using the LIF-PIV, shadowgraph, and chemiluminescence techniques

O.A. Kuti [a],[*] , K. Nishida [b]

[a] Department of Engineering, Manchester Metropolitan University, Manchester, M1 5GD, UK
[b] Department of Mechanical System Engineering, Hiroshima University, Higashi- Hiroshima, 739-8527, Japan

ARTICLE INFO

ABSTRACT

In this study, WCO biodiesel and conventional diesel fuels were characterized fundamentally in the context of their spray, gas entrainment, and combustion characteristics under diesel-like engine conditions. This was achieved using laser-induced fluorescence and particle image velocimetry (LIF-PIV), shadowgraph, and chemiluminescence techniques under non-evaporating, evaporating, and reacting conditions. The impact of fuel injection pressure and nozzle diameter on spray and gas entrainment characteristics of the fuel were also investigated. Due to higher viscosity and surface tension, it was observed that WCO biodiesel produced longer spray penetration and narrower spray angle than diesel fuel under non-evaporating conditions. Furthermore, the quantity of gas entrained by WCO biodiesel spray was lower. Due to higher distillation temperature and less gas entrainment, the WCO biodiesel liquid length was longer. The combined effect of ultra-high injection pressure of 300 MPa with a smaller nozzle hole diameter of 0.08 mm was observed to enhance gas entrainment processes. Due to its higher cetane number, WCO biodiesel displayed a shorter ignition delay. While higher injection pressure influenced the combustion processes, with less air entrained upstream of the WCO biodiesel lifted flame, it was observed that fuel oxygen content played a crucial role in its soot formation.

1. Introduction

The diesel engine is a power source for light and heavy-duty transportation and power generation applications. However, emissions from these applications are detrimental to health and the environment [1]. In achieving a low-carbon economy, stringent emission regulations are being proposed by policymakers for automakers and power generation industries [2]. Currently, heavy-duty diesel engine operates between injection pressures of 200 to 250 MPa and there are prospects of going above this level [3]. Previous works have reported that by increasing injection pressure to 300 MPa, emissions such as particulates can be reduced drastically in diesel engines [4]. In addition, the prospects of using biodiesel fuel as an alternative to achieving emission reductions in diesel engines have been reported [5]. With the notions of feedstock competing with food supply, there have been concerns about biodiesel production [6]. The key solution to mitigating this competition is recycling used cooking oil from food industries, restaurants, and sewage fatbergs. By using these waste materials, the feedstock will be made

available easily while the production of waste cooking oil biodiesel through the esterification processes will be enhanced sustainably. To mention a few, there have been several works on the prospects of using WCO biodiesel in diesel engines. WCO biodiesel has been found to produce low levels of noxious emissions such as hydrocarbon (HC) and carbon monoxide (CO) with similar engine performance when compared to diesel [7,8]. Smoke emissions have been observed to decrease with an increase in biodiesel concentration with no significant change in engine efficiency when two different cases of WCO-diesel blends were investigated [9]. It was concluded that WCO was better at reducing HC, CO, and smoke emissions as injection pressure increased. The performance, emission, and combustion characteristics of a single-cylinder diesel engine fuelled with WCO-diesel blends at various volumetric concentrations were investigated in the work reported by [10]. As the compression ratio increased, it was observed that WCO-diesel blends tend to have longer ignition delay, maximum rate of pressure rise, lower heat release rate, and higher mass fraction compared to conventional diesel fuel. The use of an optical diesel engine test rig to investigate the spray,

---

* Corresponding author.
E-mail addresses: o.kuti@mmu.ac.uk (O.A. Kuti), nishida@mec.hiroshima-u.ac.jp (K. Nishida).

combustion, and emission characteristics of neat WCO biodiesel and diesel has been reported by [11,12]. It was observed that WCO biodiesel exhibited longer liquid penetration length and a narrower spray angle than diesel. Due to poor atomization, WCO displayed longer ignition delay with a slightly lower peak of in-cylinder pressure and heat release rate than diesel with a reduction in carbon monoxide, unburned hydrocarbon, and particulate matter emissions. Fundamental studies using the constant volume vessel to investigate the spray characteristics of diesel fuel blended with hydrogenated catalytic biodiesel from WCO have been reported in [13]. It was observed that as the quantity of WCO increased in the diesel blends, the fuel density increased, and this further led to a longer liquid length. The air entrainment characteristics of fuels provide crucial information on liquid break up, mixture formation, vaporisation, and subsequently combustion processes. However, with all the previous work on biodiesel spray combustion, there is still a dearth of information on air entrainment processes in WCO biodiesel sprays, especially under diesel engine conditions. Furthermore, the role of fuel properties such as viscosity, density, and fuel oxygen content in spray formation, and combustion processes of WCO biodiesel needs further and detailed investigation. The work by [14] provided information on the air entrainment characteristics of biodiesel however it was numerical without experimental validations. Furthermore, injection conditions were not representative of real and future diesel engines. Ulu and co-workers [15] investigated the air entrainment characteristics of biodiesel fuel derived from various biomass resources under diesel engine conditions using empirical equations presented in the work reported in [16] without validations with experimental data. Riess and co-workers [3] investigated the air entrainment of biodiesel with other fuels using analytical methods without validating the results with experimental data. The work by [17,18] reported the state-of-the-art of influence of fuel properties such as cetane number and oxygen content and fuel chemical structure on biodiesel and diesel combustion. However, the underlying phenomenon through detailed fundamental experimental studies using optical diagnostics was not established. Since there is a keen interest in the use of low-carbon fuels such as WCO

biodiesel in heavy-duty combustion systems, it becomes imperative to have an in-depth understanding of its spray characteristics and air entrainment processes as compared to conventional diesel fuel. This will entail using fundamental experimental techniques such as the laser Induced Fluorescence- Particle Image Velocimetry (LIF-PIV) and high-speed video shadowgraph techniques. The subsequent combustion process that proceeds spray formation need to be studied using chemiluminescence techniques. Therefore, the novelty of this work is the use of fundamental experimental techniques to identify the role fuel properties such as surface tension, viscosity, and density play on spray formation and gas entrainment characteristics of WCO biodiesel compared to conventional diesel. The application of analytical methods to investigate and identify the impact of fuel oxygen against gas entrainment on WCO biodiesel combustion is considered novel. The influence of injection conditions such as nozzle orifice size and injection pressure on these processes are investigated. Lastly, the synergies that exist among spray formation, air/gas entrainment, and combustion processes in WCO biodiesel and diesel fuel using a high-pressure rig with optical access and diagnostics techniques will be established.

2. Experimental set-up

Experiments to investigate spray formation and combustion characteristics of waste cooking oil (WCO) biodiesel and diesel fuels were done in a high-pressure constant volume vessel presented in Fig. 1. Similar conditions to the real production diesel engine at −10° ATDC (After Top Dead Centre) were maintained inside the high-pressure constant vessel. The high-pressure vessel is set up to operate mainly on fuel-air interactions under turbulent conditions initiated at high injection conditions towards the top dead centre without considering other processes such as spray swirl, spray squish, and spray-piston interactions. The LIF-PIV (Laser-Induced Fluorescence-Particle Image Velocimetry) optical diagnostic tool in Fig. 1 was used to characterize the fuels' spray formation and gas entrainment characteristics at non-evaporating conditions. In tracking the gas entrained in the spray,
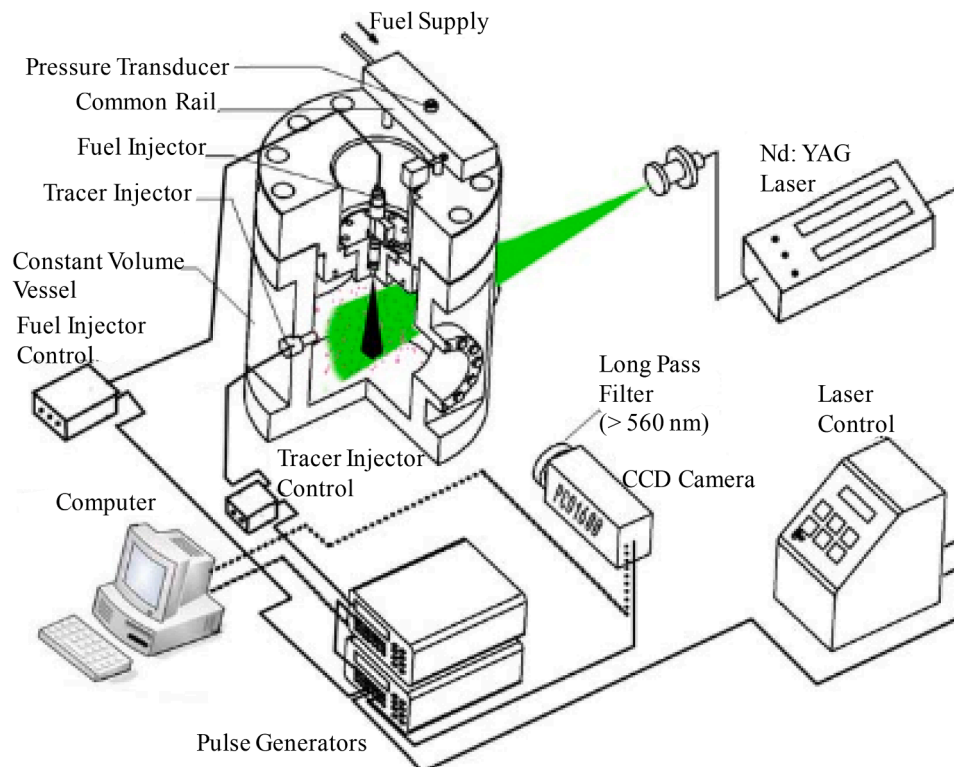

Fig. 1. Experimental set-up consisting high-pressure constant vessel with the LIF-PIV optical diagnostic system.

Rhodamine B - water solution was injected from the side of the vessel. Spray propagation images were through the elastic scattering of droplets by laser beam.

In applying the LIF-PIV technique, a double pulsed Nd:YAG laser (New Wave Research, DPIV-N50) at a wavelength of 532 nm and energy of 120 mJ was used to image the developed fuel spray and also the fluorescent images of the tracer droplets. A laser sheet of 1 mm thickness was generated with a cylindrical convex lens. The Rhodamine B solution was injected by a swirl-type injector at 9 MPa into the injected spray region in the constant volume vessel. The fuel was injected when the size of the tracer droplets being excited by the laser light reached an optimum size suitable to track the entrained gas. Two continuous images (tracer and spray images) were captured within a short interval using a CCD (Charge Coupled Device) camera (PCO 1600-PIV). The resolutions of the images were 1600 by 1200 pixels. A long pass filter which allows light of wavelength longer than 560 nm was fitted to the front of the CCD camera to only capture the fluorescence signal of the tracer droplets. The ambient pressure inside the constant volume vessel and tracer accumulator were respectively controlled using a regulator and nitrogen cylinder. Two delay generators (DG535 Stanford Inc.) were synchronized to produce electrical pulses for tracer injection, fuel injection, laser firing, and image capturing. To achieve proper distribution and optimum size for the Rhodamine B droplets, the interval between the tracer and fuel injections was maintained at 1400 ms. In addition to the LIF-PIV setup, the LDSA (Laser Diffraction Size Analyzer) optical system was used to determine the optimum tracer droplet size suitable to track the gas entrained. In predicting the magnitude of the velocity of the gas entrained in the spray, the interrogation window size of 16 by 16 pixels (1.55 by 1.55 mm) with 50 % overlap and frame time interval. The cross-correlation method was selected as the algorithm for the vector analyses in the double frame/double exposure mode. The two-dimensional ambient gas flow field was calculated based on the displacement of the tracer in the two images by using commercial PIV analytical software (Koncerto, Seika Inc.). Details about the LIF–PIV techniques and LDSA techniques for the determination of the tracer size suitable for tracking the gas entrained in the sprays can be found in previous works by some of the authors [19,20]. To eliminate the effect of shot-to-shot variations, data were acquired from 10 fuel injections. The velocity measurements were then obtained by averaging data from 5 injections with less error vector. In understanding the impact of the gas-entrained, evaporating sprays with combustion experiments were performed using the high-speed camera (FASTCAM-APX RS, Photron Corp.). Shadowgraph through Mie Scattering techniques was used to investigate the evaporating sprays. The Xenon lamp with two reflecting mirrors was utilized to illuminate the evaporating sprays. The OH (hydroxyl) chemiluminescence optical technique was used to investigate the autoignition processes and lifted flame structures through the UV-Nikkor lens (Nikon, 105 mm, f/4.5) mounted to the image intensifier (LaVision Inc., HS-IRO) connected to the high-speed camera. The OH band-pass filter of wavelength 313 nm (10 nm FWHM) coupled to the UV-Nikkor lens was used to observe the reacting sprays. To investigate the soot propensity of the reacting sprays, the two-colour pyrometry technique was used. A visible lens (Nikon, 105 mm, f/4.5) was mounted to the high-speed camera. The two-colour system was calibrated using a tungsten lamp (Polaron Components) before it was used to capture two raw identical flame images at wavelengths of 650 and 800 nm (10 nm FWHM). The Thermera HS4 software (Mitsui Optronics, version 4.61) was used to process the captured raw image data to generate two-dimensional and line-of-sight false-colour maps of soot concentration. Details about the evaporating spray combustion experiments could be found in previous works by the authors [21]. The injector used is a single-hole type with a nozzle length of 1.2 mm and sac volume of 0.488 mm^3. The injection system is a manually operated piston screw pump (High-Pressure Equipment Co. Model 37–5.75.60). It was designed with the capability of generating injection pressure up to 300 MPa in the common rail. The injector was electronically controlled by an injector driver, while the common rail pressure was measured with a pressure transducer. A pulse generator (Stanford Inc. DG 535) was used to synchronise the operation of the high-speed camera and injection system. An ambient density of 15 kg/m^3 was used to simulate engine conditions at a crank angle of $-10°$ ATDC. In investigating the effect of injection pressures on spray and combustion, three injection pressures (100, 200, and 300 MPa) were utilized. Two fuel injector nozzles with diameters of 0.16 mm (baseline) and 0.08 mm were selected for the experiments. For the spray experiments, ambient temperature of 293 K and pressure of 1.4 MPa (non-evaporating) were maintained in the constant volume vessel. For the evaporating sprays and combustion experiments the ambient temperature and pressure were maintained at 885 K and 4.0 MPa. Nitrogen which has similar properties to air was utilized for the spray experiment to create a non-reactive environment inside the constant volume chamber. For the combustion experiments, the constant volume vessel was filled with air (21 % oxygen gas). Table 1 shows the list of the experimental conditions, while Table 2 presents the physical and chemical properties of the WCO biodiesel and conventional diesel fuels.

In quantifying the amount of air entrained upstream of the lifted flame, the model by Naber and Siebers [22] presented in Eq. (1) was used.

$$\phi = \frac{2(A/F)_{st}}{\sqrt{1 + 16\left(\frac{L_o}{x^+}\right)^2} - 1} \tag{1}$$

where ϕ is an expression for the cross-sectional local equivalence ratio, at an axial location L_o(autoigntion location and flame lift of length) in a combusting fuel jet. The ϕ values provide information about the quantity of air entrained in forming reacting mixtures. The term, x^+ is a characteristics length scale for the fuel jet while $(A/F)_{st}$ is the stoichiometric air fuel ratio by mass which can be obtained by using the carbon, hydrogen, and oxygen contents as obtained in Table 2. For WCO and diesel, $(A/F)_{st}$ have values of 12.61 and 14 respectively. Details on x^+ can be found in previous work [21]. In addition, works by [23] have shown that the equivalence ratio is not a valid parameter to define the relationship of oxygenated fuel with an oxidizer in terms of its mixture stoichiometry. Therefore, the oxygen ratio, Ω, proposed in [23] defined in Eq. (2) was used to define the impact of fuel oxygen.

$$\Omega = \frac{n_O}{2n_C + \frac{1}{2}n_H} \tag{2}$$

where n_O, n_C and n_H are the number of oxygen, carbon, and hydrogen atoms respectively in the stoichiometry chemical reactions taking into

Table 1
Fundamental experimental conditions.

	Spray		Combustion		
Ambient conditions					
Density (kg/m^3)	15 ($-10°$ ATDC)				
Pressure. $P_{amb.}$ (MPa)	1.36 (non-evaporating), 4.0 (evaporating)		4.0		
Temperature, $T_{amb.}$ (K)	295 (non-evaporating), 885 (evaporating)		885		
Ambient gas	Nitrogen		Air		
Injection conditions					
Nozzle diameter, d_o (mm)	0.08, 0.16		0.16		
Fuel Pressure, P_{inj} (MPa)	100, 300		100,200,300		
Duration, $t_{inj.}$ (ms)	2.2 (non-evaporating), 1.5 (evaporating)		1.5		
Injection quantity (g/s)	d_o = 0.08 mm		d_o = 0.16 mm		
	100 MPa	**300 MPa**	**100 MPa**	**200 MPa**	**300 MPa**
WCO biodiesel	1.64	2.85	14.21	16.7	19.1
Diesel	1.61	2.5	14.2	16.5	19

Table 2
Physical and chemical properties of fuels.

Fuel property	WCO biodiesel	Diesel
Density @ 15°C (kg/m^3)	885	830
Viscosity @ 40°C (mm^2/s)	4.45	3.36
Surface tension @ 20°C (mN/m)	33.1	30.6
Cetane number	51	45
Distillation temperature (°C)	360	320
Heating value (MJ/kg)	39.03	43.1
Sulphur content (ppm)	<3	<19
Carbon content (wt. %)	77.9	86.1
Hydrogen content (wt. %)	12.0	13.8
Oxygen content (wt. %)	10.1	<1

consideration the elemental composition of both fuels in Table 2. Eq. (2) is valid if the product of the stoichiometry reaction is considered saturated stoichiometry products (SSP). Carbon dioxide, water, and molecular nitrogen are typical examples of SSPs in combustion reactions.

3. Results and discussion

3.1. Sauter mean diameter (SMD)

In evaluating the impact of the fuel types and injection conditions on atomization processes, the average spray droplet size was estimated using the Sauter mean diameter (SMD) empirical model in Eq. (1) which has been reported in [24].

$$SMD = d_o * 0.38Re^{0.25} * We^{-0.32} * \left(\frac{\mu_f}{\mu_g}\right)^{0.37} * \left(\frac{\rho_f}{\rho_g}\right)^{-0.47} \quad (3)$$

where, d_o is the nozzle diameter, Re is the Reynolds number of nozzle flow, We is the Weber number of the nozzle flow, μ_f and μ_g are fuel and gas viscosities respectively, ρ_f and ρ_g are fuel and gas densities respectively. The empirical equation is dependent on fluid flow and break-up parameters such as the Reynolds and Weber numbers. The variation of the droplet size with injection conditions and fuel types is presented in Fig. 2.

At 0.08 mm, for both fuels, spray break up and atomization were enhanced with the droplet size decreasing as injection pressure increased from 100 to 300 MPa. As the nozzle size decreased from 0.16 mm to 0.08 mm at 100 MPa, for both fuels, spray droplet size decreased resulting in the enhancement of the atomization processes. Furthermore, at all injection conditions, WCO tends to produce bigger droplets compared to diesel. As observed in the work presented in [25], the impact of fuel properties such as higher surface tension, viscosity, and
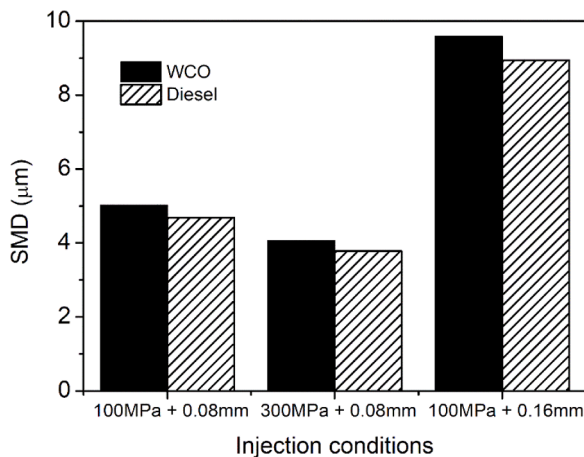

Fig. 2. Variation of droplet sizes with injection conditions for WCO biodiesel and diesel fuel sprays.

density have contributed to WCO sprays demonstrating larger droplet sizes. It could be observed that the combined injection conditions of 300 MPa and 0.08 mm had a huge impact on the droplet sizes of both fuels.

3.2. Non-evaporating spray characteristics

The line-of-sight spray morphology with gas entrainment velocities of the WCO and diesel fuels obtained through the LIF-PIV experiments are presented in Fig. 3.

For clarity, an enlarged form of the spray with gas entrainment flow field is presented. It could be observed that as the spray propagates downward, the surrounding gas moved along creating an entrainment effect towards the upstream part. For both fuels, at 0.08 mm, the sprays penetrate further downstream as injection pressure increased to 300 MPa. Furthermore, at an injection pressure of 100 MPa, the sprays penetrate further downstream as nozzle diameter increased to 0.16 mm. With further analyses of the images in Fig. 3, temporal variations in the spray tip penetrations and velocities are presented in Fig. 4. For the 0.08 mm nozzle, as injection pressure increased to 300 MPa, the spray penetrated further thereby leading to an increase in injection flow velocity. As a result of an increase in spray momentum (higher fuel mass), at 100 MPa, an increase in the nozzle diameter to 0.16 mm led to increasing spray tip penetration for both fuels. It could also be observed that spray tip penetration at 100 MPa using the 0.16 mm nozzle is longer than that at 300 MPa with the 0.08 mm nozzle. Irrespective of the fuel injection conditions as time proceeds WCO biodiesel tends to produce longer spray tip penetration compared to diesel. The WCO biodiesel viscosity and density which is about one and a half times of diesel could have played a major role in the atomization process thereby leading to longer spray penetration. For WCO biodiesel, at an injection pressure of 100 MPa and nozzle size of 0.08 mm, the spray tip penetration decreased slightly towards the end of injection (EOI). The reason for this necessitates further investigation. The spray tip velocity which was derived by finding the first order derivative of the temporal spray tip penetration is also presented in Fig. 4. It could be observed that spray tip velocity decreased with time after the start of injection (ASOI). Considering the effect of injection conditions and fuel types, the spray tip velocity followed a similar trend as the spray penetration with higher values for the WCO biodiesel at all injection conditions. Furthermore, the spray tip velocity is higher than the surrounding gas velocity presented in Fig. 2 which is about 3m/s maximum. The spray surface area for both fuels is presented in Fig. 5.

For the 0.08 mm nozzle, it could be observed that as injection pressure increased to 300 MPa, the spray surface area increased. Furthermore, by increasing the nozzle size to 0.16 mm, the spray surface increased at the 100 MPa conditions. At 100 MPa, the spray surface area of the 0.16 mm nozzle is larger compared to that of 0.08 mm at 300 MPa. For both fuels, there was no significant difference in the spray surface area at 100 MPa with the 0.08 mm nozzle. However, as the injection pressure increased to 300 MPa at 0.08 mm and nozzle size increased to 0.16 mm at 100 MPa, the spray surface area of diesel fuel tends to be larger than WCO, especially at the latter part of the spray development. On the other, the level of spray dispersion characterised by the spray angle is also presented in Fig. 5. The spray angle was obtained using the method described in previous work [19] by drawing lines from the nozzle tip touching the spray periphery at 60 % of the spray tip penetration forming a right-angled triangle. It can be observed that for the 0.08 mm nozzle, the spray angle increased for both fuels as injection pressure increased to 300 MPa. Furthermore, at 100 MPa as the nozzle size increased from 0.08 to 0.16 mm, the spray angle increased for both fuels. Compared to the nozzle size, it can be deduced that injection pressure had a significant impact on spray dispersion. As a result of higher fuel viscosity and density, at all injection conditions, WCO sprays tend to disperse less by producing narrower spray angles. The wider dispersion of diesel spray could have contributed to the larger surface area when injection pressure increased to 300 MPa at 0.08 mm nozzle
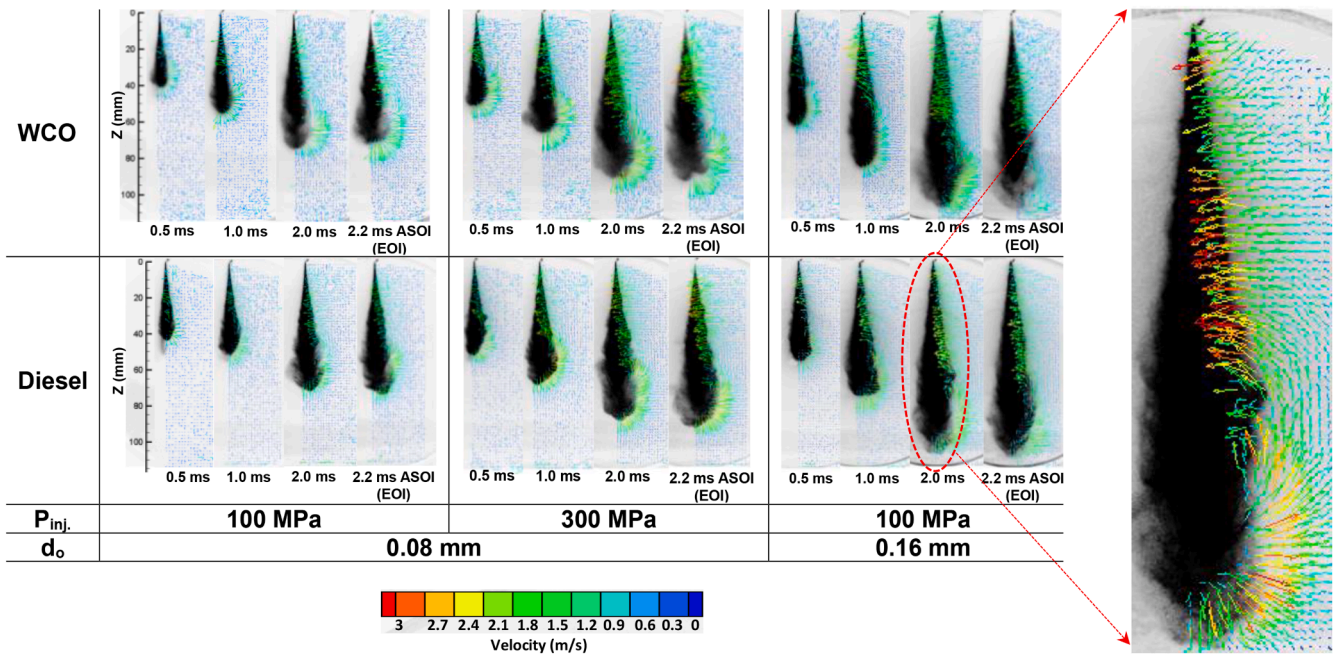
Fig. 3. Temporal variations in spray geometry and velocity distributions of ambient gas around spray for WCO biodiesel and diesel fuels at different injection conditions.
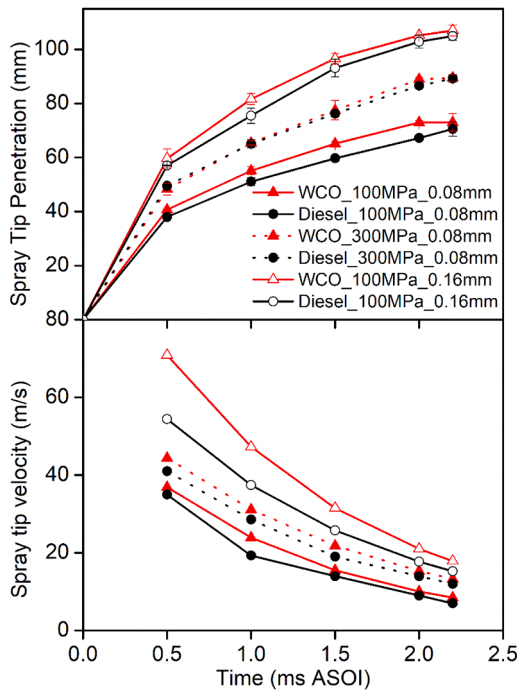

Fig. 4. Temporal variations in spray penetration and spray tip velocity for WCO biodiesel and Diesel fuel sprays.

and nozzle size increased to 0.16 mm at 100 MPa injection pressure.

3.3. Gas entrainment characteristics

The schematic diagram of the gas entrainment and recirculation with spray-capturing sections can be identified in Fig. 6.

With reference to the ambient gas, the side periphery of the spray is associated with the entrainment and recirculation sections while the hemispherical tip periphery of the spray lies at the capturing section.
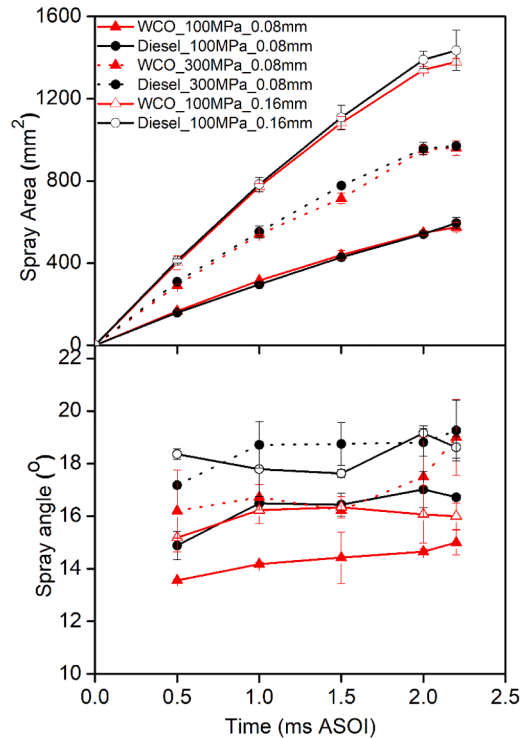

Fig. 5. Temporal variations in spray area and spray angle for WCO biodiesel and diesel fuel sprays.

From the schematic diagram, it could be noted that the recirculated gas constitutes the gas entrained at the spray periphery close to the injector.

With a fully developed spray at 2.0 ms ASOI, further data analyses using the schematic diagram produced the normal velocity component, v_n of the ambient gas distribution in Fig. 7.

In Fig. 7, the region of gas entrainment via the spray side periphery is characterized by a negative velocity distribution pattern. The gas
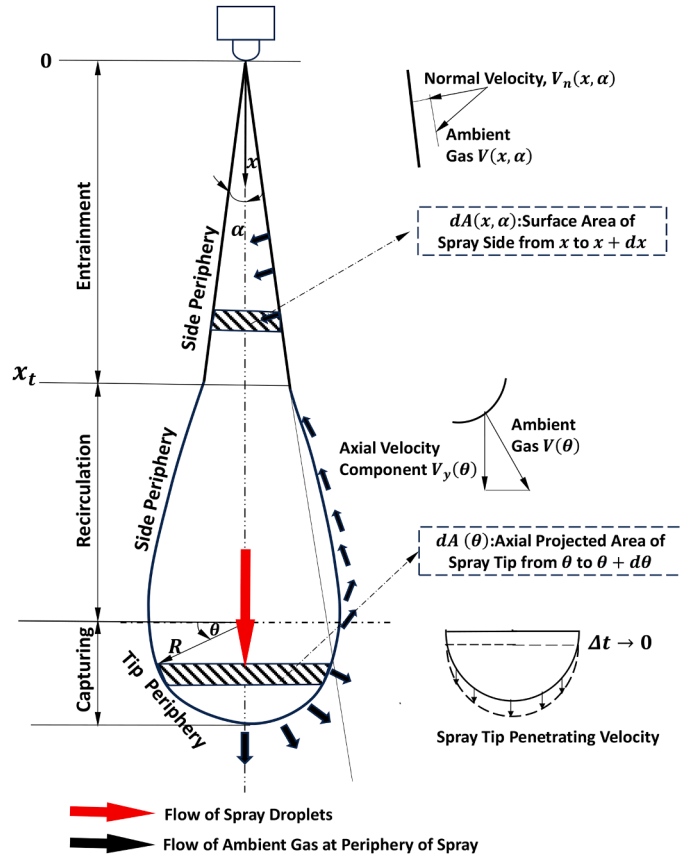
Fig. 6. Definition of velocity components and sections around spray side and tip periphery.

Fig. 7. Spatial variation of normal velocity component of ambient gas at side periphery at 2.0 ms ASOI for WCO biodiesel and diesel fuel sprays.

entrained at the side periphery of the spray increased from the injector location and reached maximum further downstream. After reaching a maximum, the normal velocity declined further downstream of the side periphery before reaching zero. A recirculation region can also be identified in Fig. 7, where the gas velocity increased from zero reaching a maximum positive value before declining to zero further downstream towards the spray tip. The location where the recirculated gas reaches a zero-velocity value towards the spray tip is taken as the region of up-ward gas entrainment towards the injector location. It can be observed as injection pressure increased up to 300 MPa, the ambient gas normal velocity increased. This observation can be attributed to the increase in the spray momentum which was transferred to the entrained gas. Furthermore, the 0.08 mm micro-hole nozzle produced lower entrained gas velocity as compared to the 0.16 mm nozzle. This could be due to the smaller spray droplets by the 0.08 mm nozzle which produced lower momentum that was transferred to the surrounding entrained gas. Due to the larger droplet size exhibited by WCO at all injection pressures, the entrained gas velocity was much lower than diesel. The WCO higher SMD values led to larger droplet sizes limiting the interaction of the spray plume with the surrounding gas at narrower regions. As a result of enhancement in the atomization process and increase in spray momentum, the combined effect of 300 MPa with 0.08 mm led to a higher normal velocity of ambient gas. Further downstream of the spray side periphery, the variation of the axial gas velocity, v_y with the angle, θ (in radians) subtended at the hemispherical section of the spray tip is presented in Fig. 8. It could be observed that the gas entrained at the spray tip increased (negative values) reaching a maximum as the hemisphereical angle increased to a certain value. However, as the hemispherical angle increased further the entrained gas decreased (reaching positive values) towards the recirculation region. At maximum, the axial velocity of the entrained gas at the spray tip is highest at 100 MPa with the 0.16
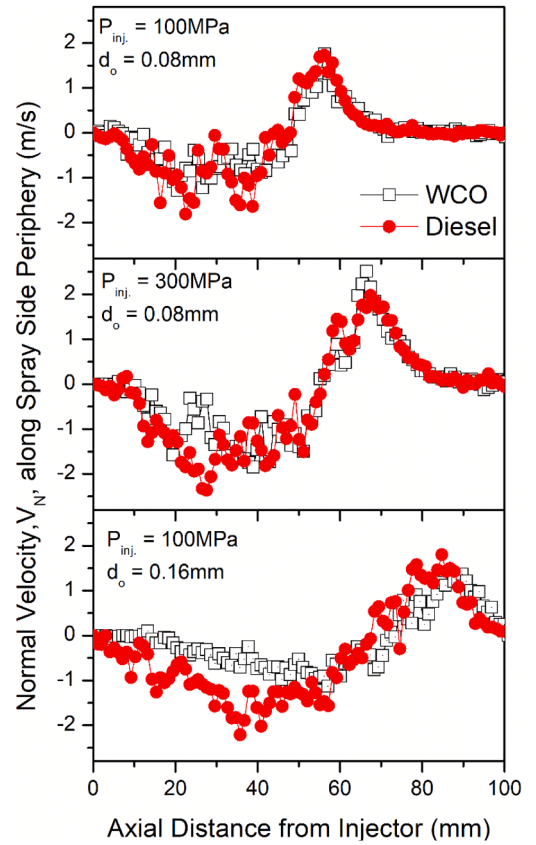
mm nozzle. As presented in Fig. 8 this observation can be attributed to the highest spray tip velocity exhibited by the 0.16 mm nozzle at 100 MPa. The spray tip velocity exhibited by 0.16 mm and 100 MPa led to an increase in momentum exchange thereby increasing the velocity of the gas entrained as the spray penetrates downstream. Since diesel spray exhibits smaller droplets at all injection conditions, the maximum axial gas velocity is higher. The total entrained gas in the WCO and Diesel sprays can be analysed using the normal and axial velocity data earlier presented in Figs. 7 and 8.

The total mass flow rate of the gas entrained, $\dot{m}_{a_{entrained}}$ via the side periphery can be defined as,

$$\dot{m}_{a_{entrained}} = \int_{0}^{X_1} \rho_a . v_n(x, \alpha) . dA(x, \alpha) \tag{4}$$

At a point of the spray tip hemispherical (tip periphery) with radius, R measured from the center at an angle θ, as the spray propagates, some quantity of surrounding gas is captured while some are pushed further downstream. Hence the total mass flow rate for the pushed gas, $\dot{m}_{a_{tip,pushing}}$ can be defined as,

$$\dot{m}_{a_{tip,pushing}} = \int_{0}^{\theta_1} \rho_a . v_y(\theta) . dA(\theta) \tag{5}$$

For the entire spray tip hemispherical (tip periphery) region with radius R, the gas entrained during spray penetration, $\dot{m}_{a_{entire\ hemisphere}}$ is defined as,

$$\dot{m}_{a_{entire\ hemisphere}} = \pi R^2 \rho_a . v_{entire\ hemisphere} \tag{6}$$

From Eqs. (3) and (4), the effective gas captured at the spray tip, $\dot{m}_{a_{captured}}$ is defined as,
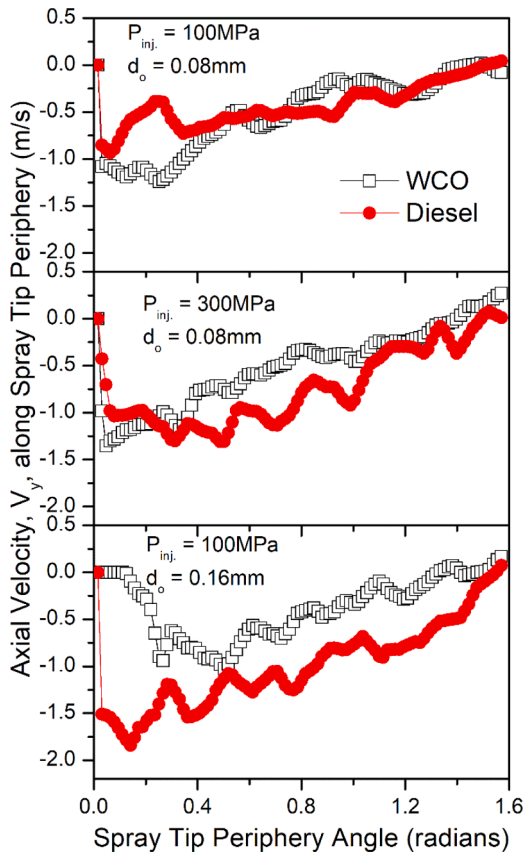
Fig. 8. Axial velocity component of ambient gas along spray tip periphery/hemispherical region at 2.0 ms ASOI for WCO biodiesel and diesel fuel sprays.

$$\dot{m}_{a_{captured}} = \dot{m}_{a_{entire\ hemisphere}} - \dot{m}_{a_{tip.pushing}} \qquad (7)$$

Therefore, the total mass flow rate of the gas entrained by the spray can be calculated as,

$$\dot{m}_{a_{total}} = \dot{m}_{a_{entrained}} + \dot{m}_{a_{captured}} \qquad (8)$$

With Eq. (6) the temporal variation of the total gas entrained by the spray is presented in Fig. 9.

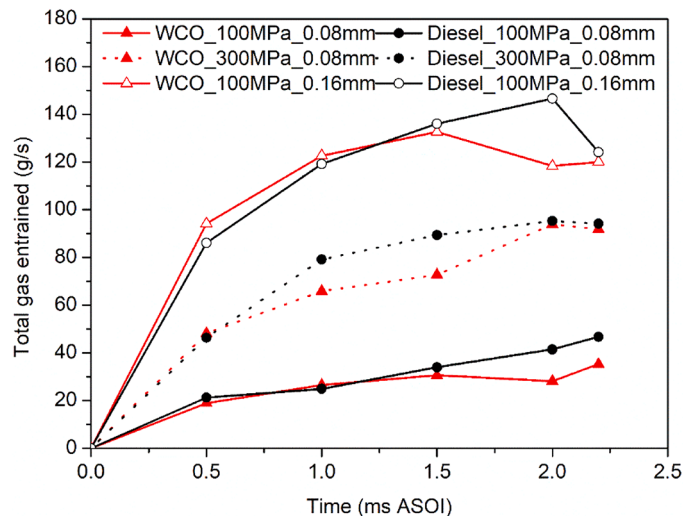In Fig. 9, as the spray propagates, the total mass flow rate of the gas

entrained increases with time and declines towards the end of injection, especially at 100 MPa with 0.16 mm and 300 MPa with 0.08 mm. As a result of the larger spray area, the total mass flow rate of the gas entrained is higher for the 100 MPa with 0.16 mm followed by 300 MPa with 0.08 mm. As a result of superior atomization processes leading to a larger spray angle, at all injection conditions, the total mass flow rate for diesel fuel is higher compared to WCO towards the end of injection. At 100 MPa up to 1.2 ms ASOI, the observations in Fig. 9 are similar to the work reported by the authors [14] whereby biodiesel fuel at 293 K tends to entrain more air at 80 MPa injection pressure and ambient conditions of 4 MPa. In addition, as depicted in Fig. 7, the higher axial velocity of air entrained into the spray core (a region expected to be closer to the injector upstream) for diesel is similar to what was reported in [14]. However, the authors [14] did not investigate higher injection conditions like the 300 MPa reported in this work. Furthermore, the observations in this study in the context of spray and gas entrainment characteristics for both fuels follow the trend reported in [15] at all injection conditions.

To investigate the effectiveness of the fuel type and injection conditions on gas entrainment, the total mass flow rate of gas entrained was normalized with the fuel mass flow rate at 2.2 ms ASOI (EOI) in Fig. 10.

It can be observed in Fig.10, that both smaller nozzle size and higher injection pressure led to increasing normalized mass flow rate of gas. Furthermore, for both fuels, the combined effect of the 300 MPa injection pressure with 0.08 mm played a vital role in gas entrainment. Due to lower viscosity, density, and surface tension, at all injection conditions, the normalized total gas mass flow rate for diesel is higher compared to WCO.

3.4. Evaporating spray

At 1.4 ms ASOI, the line-of-sight liquid phase images of the vaporising spray are presented in Fig. 11. Further analyses using image processing techniques yielded the liquid length data presented in Fig. 12.

It could be observed that after an initial liquid spray development period, the tip of the liquid phase fuel region reached a steady state condition and fluctuated about a mean axial location due to turbulence. Furthermore, the impact of gas entrainment at the 300 MPa injection pressure with 0.08 mm nozzle size can be identified in the vaporization processes leading to shorter liquid lengths for both sprays. At all injection conditions, both WCO produced a longer liquid length compared to diesel. The reason for this can be attributed to inferior atomization by WCO, which limited the rate of evaporation as a smaller quantity of air was entrained in the spray. In addition, the higher boiling point property of WCO with low volatility could have initiated a longer liquid phase length. This phenomenon has been observed in previous work on liquid-phase penetration length [26].
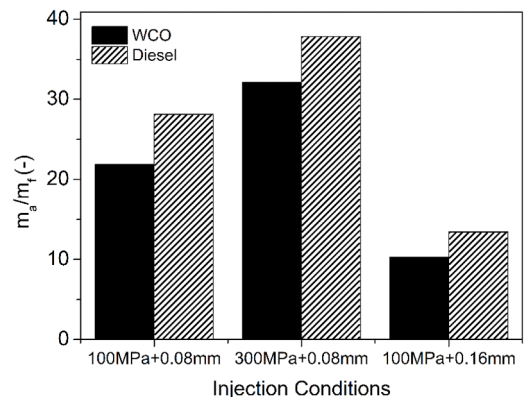

Fig. 10. Ratio of total mass flow rate of gas entrained to the mass flow rate of fuel at 2.2 ms ASOI (EOI) WCO biodiesel and diesel fuel sprays.
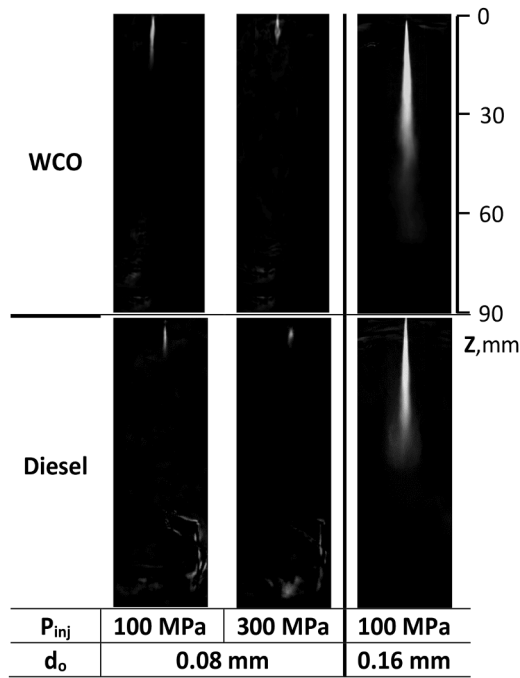

Fig. 9. Temporal variation of total gas entrained by WCO biodiesel and diesel fuel sprays at different injection conditions.

Fig. 11. Liquid phase of vaporising WCO biodiesel and diesel fuel sprays at 1.4 ms ASOI.
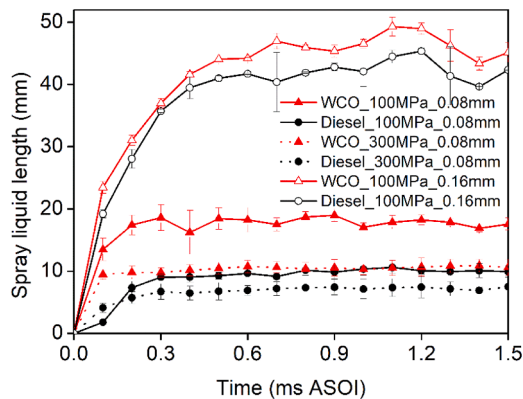

Fig. 12. Temporal variation of spray liquid length of evaporating WCO biodiesel and diesel fuel sprays.

3.5. Combustion characteristics (OH- Ignition delay and LOL and two Colour- KL factor)

The OH chemiluminescence and two-color pyrometry line-of-sight images of the combustion characteristics of WCO biodiesel are presented in Fig. 13. In Fig. 13(a), autoignition spots at high temperatures can be identified. The auto-ignition spots have been observed in previous work [1] to be formed at the location where the fuel-air mixture is rich. As a result of enhancement in mixing leading to an accelerated rate of reaction, it can be observed that an increase in injection pressure led to shorter ignition delay for both fuels. Furthermore, ignition delay timings for WCO biodiesel were shorter at all injection pressures. The cetane number and fuel oxygen content have been observed to influence the reactivity of fuels [1]. Therefore, the shorter ignition delay by WCO could be attributed to its higher cetane number and fuel oxygen content. These observations agree with previous works reported in [17,18] where rapeseed methyl ester (RME) and a biodiesel surrogate having similar fuel properties and structure to WCO biodiesel exhibited shorter ignition delay compared to conventional diesel. In Fig. 13(b) during the

fuel injection period, the flame size increased after autoignition, moved upstream towards the injector, and became quasi-steady at a location.

The distance from the injector tip to the quasi-steady location (represented by horizontal red lines) is referred to as the flame lift-off length. Upstream of the lifted flame, the air entrained plays a vital role in soot formation processes in a diesel engine. The region downstream of the flame lift-off is defined by a non-premixed zone characterized by OH radical species.

As injection pressure increased, the spray velocity increased thus making the flame structure to be pushed further pushed downstream as it stabilized.

At 100 MPa, the difference in the flame lift-off length of WCO and diesel is not significant. However, at the 200 and 300 MPa, the flame lift-off length tends to be shorter compared to diesel. The presence of a cool flame (low temperature upstream has been observed to play a vital role in the formation of a stabilized high temperature lifted flame. The cool flame is usually characterized by the formation of the formaldehyde (CH_2O) species [27,28]. The presence of the cool flame is an indication that ignition processes at low temperatures are continuously occurring within the reacting spray as fuel and air mix upstream of the lifted flame. As hot air is entrained upstream during the fuel injection period, it mixes with the cool flame thereby leading to a high-temperature ignition flame. The downstream high-temperature flame propagates upward joining the new flame to form a quasi-stable flame. The transition from a cool flame to a high-temperature-lifted flame has been reported to be influenced strongly by the fuel type [28]. Therefore, the shorter flame lift-off length observed in WCO could be attributed to the closer location of the CH_2O species to the injector. In addition, because of higher fuel density yielding a lower injection velocity and higher viscosity, WCO flame lift-off length is shorter than diesel. These observations have been reported in previous works by [29]. As presented in Fig. 13(b) (see inset), it could be observed that the local equivalence ratio decreased as injection pressure increased up to 300 MPa. This further led to more air entrained upstream while the flame reaction zone was further pushed downstream. As observed earlier in the LIF-PIV experiments, more air was entrained upstream of the flame because of the enhancement in the atomization processes during flame propagation. At all injection pressures, due to poor atomization, WCO lift-off length was shorter with a higher equivalence ratio at all injection pressure conditions signifying less gas entrainment upstream of the developed flame. In gaining a detailed understanding of the soot propensities of the fuels, the KL images obtained from the two-colour pyrometry experiments are presented in Fig. 13(c). The soot KL factor is expressed in soot number per cm². It can be observed in Fig. 13(c), that as injection pressure increased from 100 to 300 MPa, both soot quantity and area decreased. With WCO equivalence ratios higher (refer to Fig. 13(b)), the intensity of the KL contours was lower compared to diesel, especially at the 200 and 300 MPa injection pressures. This implies that WCO soot formation does not depend on the quantity of air entrained in the lifted flame. With reference to Eq. (2), the oxygen ratio of WCO biodiesel is 1.6 % while diesel fuel has a value of zero since it has no oxygen in its atom. Compared to diesel, the higher oxygen ratio is an indication that fuel oxygen played a vital role in WCO biodiesel soot oxidation despite its higher local equivalence ratio which is dependent on the entrained air. Fig. 14 presents the temporal variation of the soot quantity formed by WCO and diesel fuels. Soot quantity increased from the beginning of the combustion event towards the end of the injection period. However, after the end of fuel injection, it decreased due to the enhancement in oxidation processes.

As a result of enhancement in air entrainment, an increase in injection pressure led to a decrease in soot quantity. WCO biodiesel displayed early soot formation and produced more soot, especially at 100 MPa compared to diesel after the end of injection (AEOI). However, at a later period (about 0.75 ms AEOI), at all injection pressures, the net soot formed by WCO declined faster compared to diesel. Since WCO entrained less air compared to diesel, the reduction in net soot could be
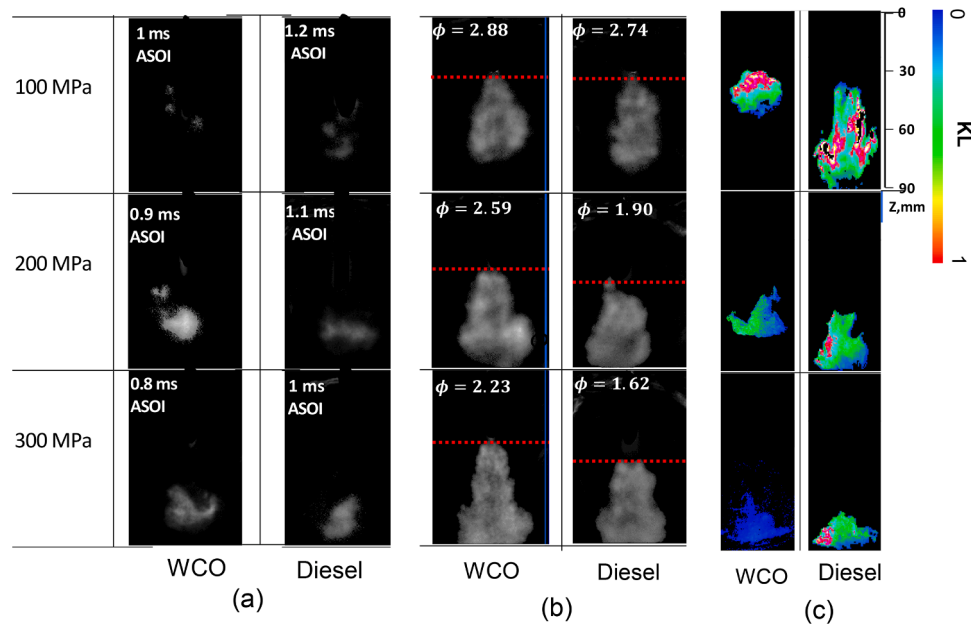
Fig. 13. Variations of (a) autoignition, (b) lifted flames during injection event (1.4 ms ASOI) and (c) soot formation (0.25 ms AEOI) with injection pressure for WCO biodiesel and diesel reacting sprays.
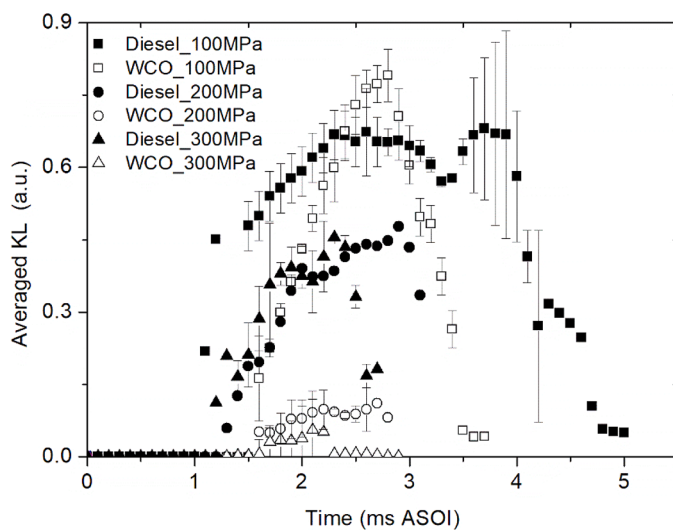

Fig. 14. Temporal variations of soot formation with injection pressure for WCO biodiesel and diesel reacting sprays.

attributed significantly to the chemical fuel-bound oxygen. Hellier et al. [30] reported that the oxygen content of a fuel has the tendency to play vital role in soot oxidation. As earlier presented in Table 2, oxygen content in WCO biodiesel is 11.1 % as against diesel which is <1 % or negligible. Therefore, as injection pressure increased, the oxygen atom in WCO could have enhanced soot oxidation during the combustion events.

4. Conclusion

In this study, the LIF-PIV, shadowgraph and chemiluminescence techniques with high-pressure rig have been used to characterize WCO biodiesel spray combustion processes under diesel engine conditions. Furthermore, the synergies that exist among spray formation, gas entrainment, and combustion processes have been established using optical diagnostic tools and analytical methods. From the LIF-PIV

experiments, it was observed that due to higher viscosity, WCO biodiesel produced, larger droplet size, longer spray penetration with narrower spray angle, and, higher spray velocity under non-evaporating conditions. Due to the inferior atomization of WCO biodiesel, the quantity of gas entrained was lower. From the shadowgraph measurements, under evaporating conditions, WCO biodiesel produced longer liquid length due to less quantity of gas entrained and higher distillation temperature. The combined effect of ultra-high injection pressure of 300 MPa with smaller nozzle hole diameter of 0.08 mm was observed to enhance gas entrainment processes. Due to the higher cetane number, WCO biodiesel combusts faster producing a shorter ignition delay duration. With less air entrained upstream of the lifted flame, from the fuel-oxygen ratio analyses, it was observed that the fuel-bound oxygen atoms in WCO biodiesel molecule played a crucial role in soot formation.

CRediT authorship contribution statement

O.A. Kuti: Writing – review & editing, Writing – original draft, Visualization, Validation, Software, Resources, Project administration, Methodology, Investigation, Funding acquisition, Formal analysis, Data curation, Conceptualization. **K. Nishida:** Supervision.

Declaration of competing interest

The authors declare that they have no known competing financial interests or personal relationships that could have appeared to influence the work reported in this paper.

Data availability

Data will be made available on request.

References

[1] O.A. Kuti, S.M. Sarathy, K. Nishida, Spray combustion simulation study of waste cooking oil biodiesel and diesel under direct injection diesel engine conditions, Fuel 267 (2020) 117240, https://doi.org/10.1016/j.fuel.2020.117240.

[2] The role of biofuels beyond 2020 commissioned by BP executive summary, in: Element Energy Limited 20 Station Road Cambridge CB1 2JD, 2013, pp. 1–30.

[3] S. Riess, L. Weiss, A. Peter, J. Rezaei, M. Wensing, Air entrainment and mixture distribution in Diesel sprays investigated by optical measurement techniques, Int. J. Engine Res. 19 (2017) 120–133, https://doi.org/10.1177/1468087417742527.

[4] O.A. Kuti, Z. Wu, K. Nishida, X. Wang, Z. Huang, Effect of injection pressure on ignition, flame development and soot formation processes of biodiesel fuel spray, SAe Int. J. Fuels. Lubr. 3 (2010) 1057–1070, https://doi.org/10.4271/2010-32-0053.

[5] O.A. Kuti, J. Zhu, K. Nishida, X. Wang, Z. Huang, Characterization of spray and combustion processes of biodiesel fuel injected by diesel engine common rail system, Fuel 104 (2013) 838–846, https://doi.org/10.1016/j.fuel.2012.05.014.

[6] C. Jin, M. Yao, H. Liu, C.F. Lee, J. Ji, Progress in the production and application of n-butanol as a biofuel, Renew. Sustain. Energy Rev. 15 (2011) 4080–4106.

[7] A. Hull, I. Golubkov, B. Kronberg, J. van Stam, Alternative fuel for a standard diesel engine, Int. J. Engine Res. 7 (2006) 51–63, https://doi.org/10.1243/146808705x30549.

[8] A.N. Ozsezen, M. Canakci, C. Sayin, Effects of biodiesel from used frying palm oil on the performance, injection, and combustion characteristics of an indirect injection diesel engine, Energy Fuels 22 (2008) 1297–1305, https://doi.org/10.1021/ef700447z.

[9] M. Lapuerta, J. Rodriguez-Fernandez, J. Agudelo, Diesel particulate emissions from used cooking oil biodiesel, Bioresour. Technol. 99 (2008) 731–740, https://doi.org/10.1016/j.biortech.2007.01.033.

[10] K. Muralidharan, D. Vasudevan, Performance, emission and combustion characteristics of a variable compression ratio engine using methyl esters of waste cooking oil and diesel blends, Appl. Energy 88 (2011) 3959–3968, https://doi.org/10.1016/j.apenergy.2011.04.014.

[11] J. Hwang, Y. Jung, C. Bae, Spray and combustion of waste cooking oil biodiesel in a compression-ignition engine, Int. J. Engine Res. 16 (2015) 664–679, https://doi.org/10.1177/1468087415585282.

[12] J. Hwang, C. Bae, T. Gupta, Application of waste cooking oil (WCO) biodiesel in a compression ignition engine, Fuel 176 (2016) (2016) 20–31, https://doi.org/10.1016/j.fuel.2016.02.058.

[13] Z. He, P. Tamilselvan, Q. Wang, H. Feng, X. Yu, Experimental study of spray characteristics of diesel/hydrogenated catalytic biodiesel blended fuels under inert and reacting conditions, Energy 153 (2018) 349–358, https://doi.org/10.1016/j.energy.2018.04.045.

[14] A.J. Ghandilou, H. Taghavifar, New insight into air/spray boundary interaction for diesel and biodiesel fuels under different fuel temperatures, Biofuels. 13 (2022) 1087–1101, https://doi.org/10.1080/17597269.2022.2105867.

[15] A. Ulu, G. Yildiz, A.D. Rodriguez, Ü. Özkol, Spray analysis of biodiesels derived from various biomass resources in a constant volume spray chamber, ACS Omega [online] 7 (2022) 19365–19379, https://doi.org/10.1021/acsomega.2c00952.

[16] C.D. Rakopoulos, D.C. Rakopoulos, E.G. Giakoumis, D.C. Kyritsis, Validation and sensitivity analysis of a two-zone Diesel engine model for combustion and emissions prediction, Energy Convers. Manage 45 (2004) 1471–1495, https://doi.org/10.1016/j.enconman.2003.09.012.

[17] R. Madihi, M. Pourfallah, M. Gholinia, M. Armin, A.Z. Ghadi, Thermofluids analysis of combustion, emissions, and energy in a biodiesel $(C_{11}H_{22}O_2)$ /natural gas heavy-duty engine with RCCI mode (Part II: fuel injection time/ Fuel injection rate), Int. J. Thermofluids 16 (2022) 100200, https://doi.org/10.1016/j.ijft.2022.100200.

[18] A. Al Ezzi, M.A. Fayad, A. Jubori, A.A. Jaber, L.A. Alsadawi, H.A. Dhahad, M.T. Chaichan, Talal Yu, Influence of fuel injection pressure and RME on combustion, NO emissions and soot nanoparticles characteristics in common-rail HSDI diesel engine, Int. J. Thermofluids 15 (2022) 100173, https://doi.org/10.1016/j.ijft.2022.100173.

[19] O.A. Kuti, K. Nishida, J. Zhu, Experimental studies on spray and gas entrainment characteristics of biodiesel fuel: implications of gas entrained and fuel oxygen content on soot formation, Energy 57 (2013) 434–442, https://doi.org/10.1016/j.energy.2013.05.006.

[20] J. Zhu, C. Shan, K. Nishida, W. Long, D. Dong, Simultaneous PIV/LIF-PIV measurements and numerical simulation of liquid flow and ambient gas flow for transient diesel spray, Fuel 309 (2022) 122211, https://doi.org/10.1016/j.fuel.2021.122211.

[21] O.A. Kuti, J. Zhu, K. Nishida, X. Wang, Z. Huang, Characterization of spray and combustion processes of biodiesel fuel injected by diesel engine common rail system, Fuel 104 (2013) 838–846.

[22] J. Naber, D. Siebers, Effects of gas density and vaporization on penetration and dispersion of diesel sprays, SAE Paper 960034 (1996).

[23] C.J. Mueller, The quantification of mixture stoichiometry when fuel molecules contain oxidizer elements or oxidizer molecules contain fuel molecules, SAE Paper 2005-01-3705 (2005).

[24] H. Hiroyuki, M. Arai, M. Tabata, Empirical Equations for the sauter meandiameter of a diesel spray, SAE Tech. Paper Series (1989), https://doi.org/10.4271/890464.

[25] C.E. Ejim, B.A. Fleck, A. Amirfazli, Analytical study for atomization of biodiesels and their blends in a typical injector: surface tension and viscosity effects, Fuel 86 (2007) 1534–1544, https://doi.org/10.1016/j.fuel.2006.11.006.

[26] D.L. Siebers, Liquid-Phase Fuel Penetration in Diesel Sprays, SAE Tech. Paper Series (1998), https://doi.org/10.4271/980809.

[27] V. Vasudevan, D.F. Davidson, R.K. Hanson, C.T. Bowman, D.M. Golden, High-temperature measurements of the rates of the reactions $CH_2O + Ar \rightarrow$ Products and $CH_2O + O_2\rightarrow$ Products, Proc. Combust. Inst. 31 (2007) 175–183, https://doi.org/10.1016/j.proci.2006.07.017.

[28] Pickett, L.M., Siebers, D.L., Idicheria, C.A. Relationship Between Ignition Processes and the Lift-Off Length of Diesel Fuel Jets. SAE Paper 2005-01-3843 (2005). https://doi.org/10.4271/2005-01-3843.

[29] D. Siebers, B. Higgins, Flame lift-off on direct injection diesel sprays under quiescent conditions, SAE Paper 2001-01-0530 (2001).

[30] P. Hellier, M. Talibi, A. Eveleigh, N. Ladommatos, An overview of the effects of fuel molecular structure on the combustion and emissions characteristics of compression ignition engines, Proc. IMechE Part D: J. Automob. Eng. 232 (2018) 90–105.